LETTER • OPEN ACCESS

OLCI-based NIR-red models for estimating chlorophyll-*a* concentration in productive coastal waters—a preliminary evaluation

To cite this article: Wesley J Moses *et al* 2019 *Environ. Res. Commun.* **1** 011002

View the underline article online for updates and enhancements.

Recent citations

- Pavel Plyaka *et al*
- Application of Sentinel 3 OLCI for chl-a retrieval over small inland water targets: Successes and challenges
  Jeremy Kravitz *et al*

Environmental Research Communications

LETTER

OLCI-based NIR-red models for estimating chlorophyll-*a* concentration in productive coastal waters—a preliminary evaluation

Wesley J Moses[1] , **Vladislav Saprygin**[2], **Victoria Gerasyuk**[2], **Vasiliy Povazhnyy**[2], **Sergey Berdnikov**[2] and **Anatoly A Gitelson**[3]

1   US Naval Research Laboratory, Washington, DC, United States of America
2   Southern Scientific Center of the Russian Academy of Sciences, Rostov-on-Don, 344 000 Russia
3   Technion—Israel Institute of Technology, Haifa, Israel

E-mail: wesley.moses@nrl.navy.mil
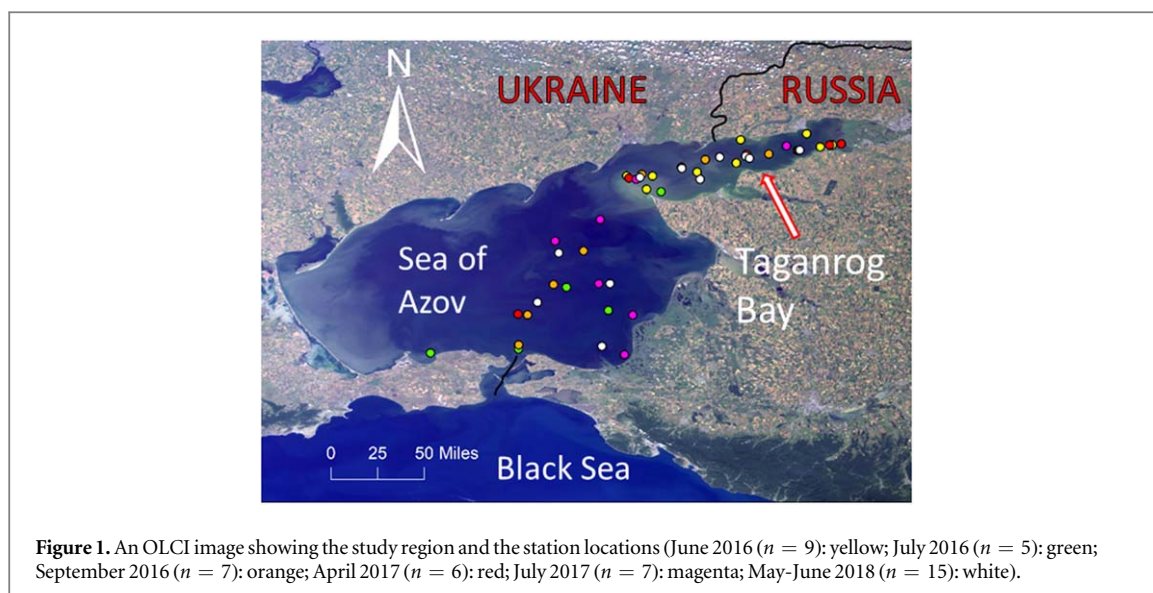
Abstract

We present here results that demonstrate the potential of the recently launched Ocean and Land Colour Instrument (OLCI) onboard the satellite Sentinel-3A to deliver accurate estimates of chlorophyll-*a* (chl-*a*) concentration in coastal waters using reflectances in the red and near-infrared (NIR) spectral regions. Two-band and three-band NIR-red models that were previously used for data from the MEdium Resolution Imaging Spectrometer (MERIS) were applied to OLCI data from the Sea of Azov and the Taganrog Bay, Russia. Atmospherically corrected reflectance data from OLCI were compared to *in situ* reflectance data collected concurrently with a field spectrometer. Results show that the default atmospheric correction procedure currently applied to OLCI data performs well in preserving the spectral shape of chl-*a*-specific reflectance features in the red and NIR regions. Similar to what was achieved with MERIS data, the NIR-red models yield accurate estimates of chl-*a* concentration, with accuracies on the order of 90%, though the parameters of the NIR-red algorithms based on OLCI data are slightly different from what was obtained with MERIS data. More data, from various geographical locations, need to be analyzed to establish robust NIR-red algorithms for OLCI data.

1. Introduction

Water quality is a key indicator of ecosystem health. The ability to detect water quality through remote sensing has greatly aided effective monitoring of ecosystem changes and has opened ways for gaining new insights into processes and ecosystem dynamics that drive the changes and also the impact of the changes. This is particularly important in coastal and inland waters that are significantly impacted by events on land.

The concentration of chlorophyll-*a* (chl-*a*), a proxy for the trophic status of water body, is a key water quality parameter and is commonly used to monitor the biophysical status of a water body (e.g., [1]). Accurately estimating chl-*a* concentration in turbid and productive coastal waters is challenging on multiple fronts. The presence of suspended sediments and colored dissolved organic matter in addition to chl-*a* makes the water-leaving radiance signal optically complex, resulting in increased difficulty in isolating chl-*a*-specific spectral features and determining chl-*a* concentration (e.g., [2]). Correcting for atmospheric effects on satellite data can be particularly difficult if sources of atmospheric pollutants, such as industrial factories, are located nearby on land, which can produce atmospheric aerosol mixtures that are very different from what is modeled in typical aerosol models (e.g., [3]). The proximity of land enhances the chances of spurious signal due to contribution from adjacent land pixels (e.g., [4]), which could be significant depending on factors such as topography and illumination/viewing geometry.

In spite of the aforementioned challenges, several algorithms have been developed and applied, with varying degrees of success, to estimate chl-*a* concentration in coastal waters [5–7]. In particular, we have previously

Figure 1. An OLCI image showing the study region and the station locations (June 2016 ($n = 9$): yellow; July 2016 ($n = 5$): green; September 2016 ($n = 7$): orange; April 2017 ($n = 6$): red; July 2017 ($n = 7$): magenta; May-June 2018 ($n = 15$): white).

developed two-band and three-band algorithms based on red and near-infrared (NIR) spectral channels of the MEdium Resolution Imaging Spectrometer (MERIS), which have consistently yielded highly accurate estimates of chl-*a* concentration for coastal and inland waters in various geographic locations using remote sensing data measured using field spectrometers, airborne sensors, and satellites, and data simulated using a radiative transfer model [8–14]. NIR-red algorithms are suitable for waters with chl-*a* concentrations high enough (upwards of 3–5 mg m^{-3} [5]) to produce discernible spectral features in the red and NIR regions of the reflectance spectrum. After MERIS ceased functioning in 2012, the European Space Agency developed its replacement, the Ocean and Land Colour Instrument (OLCI), and launched it onboard the space mission Sentinel-3A in February 2016. OLCI has all of the spectral channels of MERIS with a few additional channels. A few studies have demonstrated the potential and the challenges of retrieving reliable water quality products from OLCI data [15–17]. The goal of this study is to examine whether the two-band and three-band NIR-red algorithms can yield similar accuracies when applied to OLCI data as were previously obtained from MERIS data. Besides accuracy, we also examined the parameters of the NIR-red algorithms based on OLCI data and compared them to what were previously obtained from MERIS data. The spectral fidelity of OLCI data was also examined by comparison with *in situ* measured reflectance data.

2. Data and methods

2.1. Study area and *in situ* measurements

The study area is the same region where we had previously worked with MERIS data [12–14]—the Sea of Azov, a shallow inland sea north of the Black Sea, adjoined by Russia on the east and Ukraine on the west, and Taganrog Bay, which is located on the northeastern part of the Sea of Azov (figure 1). These water bodies are shallow, with low salinity and high influx of nutrients from several surrounding rivers that run through industrial and agricultural land, often resulting in eutrophic and hypertrophic conditions, especially in Taganrog Bay, where algal blooms are common [18–20]. We have previously [14] described the suitability of these waters for testing remote sensing algorithms for retrieving coastal water quality products.

Researchers at the Southern Scientific Center of the Russian Academy of Sciences, in Rostov-on-Don, Russia, undertook *in situ* data collection campaigns on the Sea of Azov and the Taganrog Bay in June, July, and September of 2016, April and July of 2017, and May and June of 2018. At each station, water samples were collected to determine *in situ* chl-*a* concentration. Water samples were filtered through Whatman GF/F glass filters. Chl-*a* was extracted from the filers using acetone. Chl-*a* concentration was determined spectrophotometrically using Jeffrey and Humphrey's [21] trichromatic equations.

In June 2016, besides chl-*a* concentration, the water-leaving radiance was also measured, using an S-41 spectrometer manufactured by SOLAR Laser Systems. S-41 is a miniature single-channel lens spectrometer that uses a three-lens achromat-anastigmat system for camera foreoptics. The spectrometer offers a choice of three spectral ranges of operation, namely, 200–400 nm, 390–780 nm, and 754–1140 nm. For this campaign, data were collected in the 390–780 nm range. The spectrometer uses a diffraction grating to spectrally split the incoming light, resulting in a spectral resolution of about 1.7 nm.

Above-water radiance measurements were taken by pointing the S-41 spectrometer downward towards the water surface at a viewing angle of about 40° off nadir and an azimuthal angle of 135° from the solar plane, as recommended by NASA's protocol for ocean optics measurements [22], to minimize specular reflection of solar radiation into the spectrometer. A 97% reflective Spectralon panel coated with barium sulfate was used to normalize the above-water radiance measurements and derive the remote sensing reflectance (R_{rs}). R_{rs} was calculated as follows:

$$R_{rs} = \frac{L_{w+s} - \rho(\theta)L_{sky}}{(\pi L_{ref}/R_{ref})} \tag{1}$$

where, L_{w+s} is the radiance recorded above the water, which includes radiance from the water column, the water surface, and the sky; L_{sky} is the sky radiance; L_{ref} is the radiance measured over the Spectralon reference panel; R_{ref} is the reflectivity of the reference panel; and $\rho(\theta)$ is a proportionality factor that relates the sky radiance reflected from the water surface to the sky radiance measured by pointing the spectrometer towards the sky. $\rho(\theta)$ is dependent on the direction and speed of wind, the field-of-view (FOV) of the detector, and the angular distribution of the sky radiance, and is equal to the average Fresnel reflectance over the detector FOV in the case of a calm, level water surface with a uniformly distributed sky radiance. The measurements were taken within the range of conditions for which a $\rho(\theta)$ value of 0.028 is recommended [23].

2.2. OLCI data

OLCI contains 15 spectral channels with the same spectral characteristics of MERIS and six additional channels, for a total of 21 channels spanning the 420–1020 nm range. Of the six additional channels, the channels centered at 400 nm and 1020 nm are expected to improve the ability to characterize atmospheric aerosols and correct for atmospheric effects; two channels centered at 764.4 nm and 767.5 nm, near the oxygen absorption line, are expected to improve cloud height detection; the channel at 940 nm is expected to improve water vapor retrieval; and the channel at 673 nm is expected to provide more accurate measures of chlorophyll fluorescence. Besides the additional spectral channels, other improvements in OLCI include, higher signal-to-noise ratio, finer radiometric resolution, sun-glint mitigation through camera tilt, potentially better radiometric stability, and more robust characterization of the instrument to account for stray light contamination. The spatial resolution is the same as for MERIS, at about 300 m.
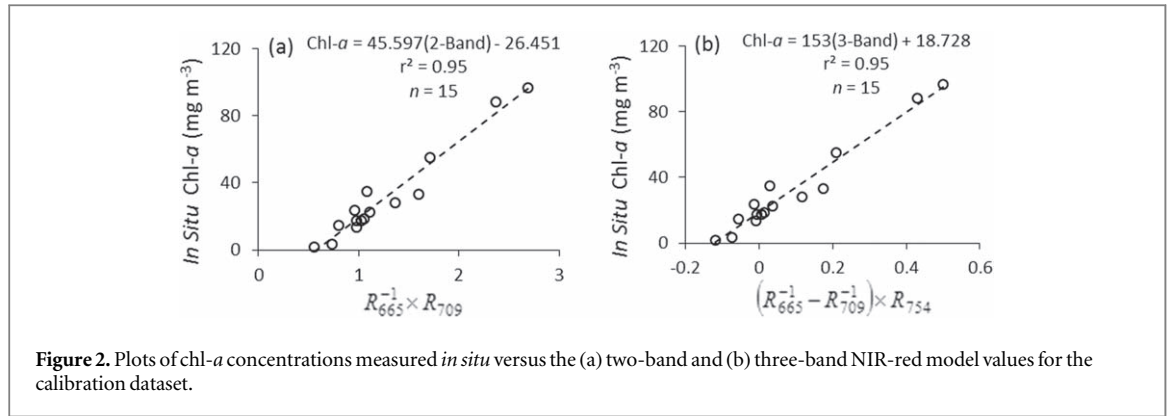
Level-2 OLCI images, containing surface reflectance data corrected for atmospheric effects, were used. Atmospheric effects were accounted for by using the same procedure that was used for MERIS, with the Bright Pixel Atmospheric Correction [24, 25] option applied to pixels classified as Case II water pixels, which included all pixels corresponding to the *in situ* stations. Even though we allowed a temporal difference of only up to two days between the *in situ* and satellite data acquisitions in our past studies [12] in this region, we relaxed it to ±3 days for this study because adding an additional day did not introduce any perceptible additional variation in the dataset as the data were collected during periods of fairly stable weather conditions and it resulted in more data points for analysis, especially in the moderate chl-*a* range. Additionally, the following criteria [12] were applied in choosing satellite pixels and the corresponding *in situ* stations for this study:

- the station is at a distance of at least two pixel lengths from the shore, to minimize adjacency effects from land.

- the pixel is free of clouds/haze.

- the atmospherically corrected surface reflectance for the pixel is not negative beyond 443 nm and up to 800 nm.

- the magnitude and spectral shape of the reflectance are typical of inland and coastal waters.

Applying the aforementioned criteria resulted in 49 data pairs. The temporal difference was zero days for 17 pairs, one day for 9 pairs, two days for 16 pairs, and three days for 7 pairs. The effect of temporal difference is a function of factors such as the local weather and storm events that could trigger rapid changes in water quality. No such events occurred during and around the *in situ* data collection campaigns.

2.3. NIR-red models

NIR-red algorithms for estimating chl-*a* concentration are based on the strong absorption by chl-*a* in the red region, around 670 nm (e.g., [26]), and the peak in reflectance in the NIR region (e.g., [27]), caused by the combined effect of progressively decreasing absorption by chl-*a* and increasing absorption by water. The position and magnitude of this peak vary as a function of chl-*a* concentration [28] and can be used to estimate chl-*a* concentration, especially in turbid and productive waters, where algorithms based on reflectance in blue and green spectral regions fail due to the spectral influence of dissolved organic matter and suspended particles

Figure 2. Plots of chl-*a* concentrations measured *in situ* versus the (a) two-band and (b) three-band NIR-red model values for the calibration dataset.

in the water column and two-band and three-band NIR-red models have provided consistently high accuracy [5, 8–14]. The two-band NIR-red model is simple in its formalism and is a straightforward division of the reflectance peak in the NIR by the reflectance trough in the red. The three-band NIR model uses a third NIR channel and attempts to explicitly account for absorption by non-algal particles by using a subtraction term to remove from the red reflectance any absorption due to non-algal particles, which is assumed to be constant at both wavelengths. The development of the NIR-red models has been discussed in detail by Dall'Olmo and Gitelson [29].Considering the locations of the OLCI spectral channels in the red and NIR regions, the OLCI-based two-band and three-band NIR-red models are,

$$\text{Two-Band OLCI Model: } \text{Chl-}a \propto [R_{665}^{-1} \times R_{709}] \tag{2}$$

$$\text{Three-band OLCI model: } \text{Chl-}a \propto [(R_{665}^{-1} - R_{709}^{-1}) \times R_{754}] \tag{3}$$

3. Results and discussion

The dataset was divided into calibration and validation datasets in order to calibrate the relationships between the OLCI-based NIR-red models and chl-*a* concentrations and test the accuracy of the resulting NIR-red algorithms. Calibration and validation datasets are often obtained by grouping all the data together, sorting them in ascending order of the magnitude of the parameter of interest, and evenly splitting them into calibration and validation datasets. However, when the data are split in this manner, the calibration dataset encompasses all spatio-temporal conditions contained in the validation dataset, rendering the validation non-independent of the calibration. Our choice of data for calibration was guided by two criteria, (i) data that span a wide range of chl-*a* concentrations and (ii) data that are temporally distinct from the validation dataset. We chose data from June 2016, which contained moderate-high chl-*a* concentrations, and April 2017, which contained low-moderate chl-*a* concentrations, for calibration. Altogether, there were 15 data points in the calibration dataset and 34 data points in the validation dataset. The minimum, maximum, median, and mean of chl-*a* concentrations in the calibration dataset were 1.81, 96.41, 22.84, and 31.34 mg m^{-3}, respectively, whereas the minimum, maximum, median, and mean for the validation dataset were 1.3, 84.27, 7.50, and 12.09 mg m^{-3}.

Both two-band and three-band NIR-red models exhibited a close relationship with *in situ* measured chl-*a* concentrations in the calibration dataset (figure 2), each with a determination coefficient of 0.95, resulting in the following OLCI-based NIR-red algorithms:

$$\text{Two-Band: } \text{Chl-}a = 45.597(R_{665}^{-1} \times R_{709}) - 26.451 \tag{4}$$

$$\text{Three-Band: } \text{Chl-}a = 153[(R_{665}^{-1} - R_{709}^{-1}) \times R_{754}] + 18.728 \tag{5}$$

The NIR-red algorithms were applied to the validation data (figure 3). The chl-*a* concentrations estimated using the two-band NIR-red algorithm had a Root Mean Square Error (RMSE) of 6.53 mg m^{-3} and a Mean Absolute Error (MAE) of 4.53 mg m^{-3}, which are 7.88% and 5.46%, respectively, of the range of chl-*a* concentrations in the validation dataset. The RMSE and MAE for the three-band NIR-red model were 7.0 mg m^{-3} and 4.58 mg m^{-3}, which correspond to 8.45% and 5.52%, respectively, of the range of chl-*a* concentrations in the validation dataset.

Except for a slight overestimation in the 20–40 mg m^{-3} range (figure 3), both algorithms yielded accurate estimates. More data need to be collected and analyzed in order to evaluate any potential systematic bias in this range. It is worth noting that the coefficients of the OLCI-based NIR-red algorithms are quite different from those for the previously published MERIS-based algorithms [12].
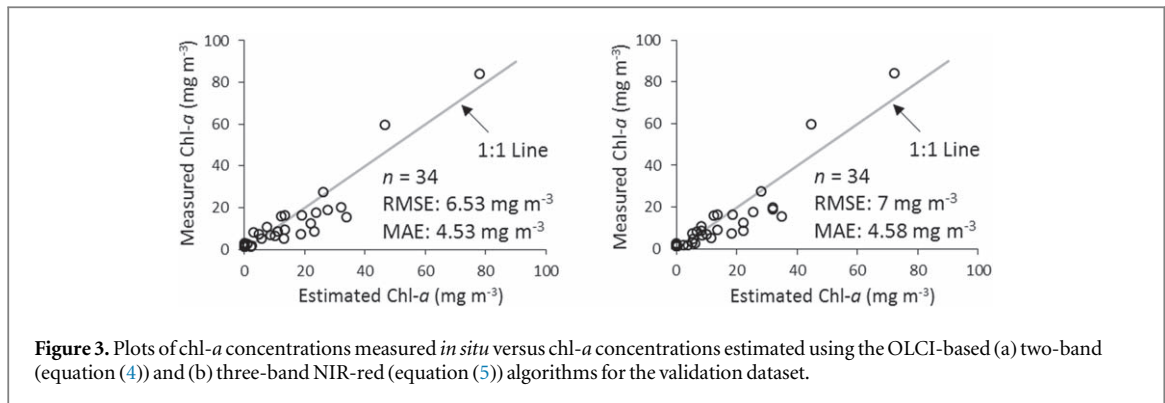
Figure 3. Plots of chl-*a* concentrations measured *in situ* versus chl-*a* concentrations estimated using the OLCI-based (a) two-band (equation (4)) and (b) three-band NIR-red (equation (5)) algorithms for the validation dataset.
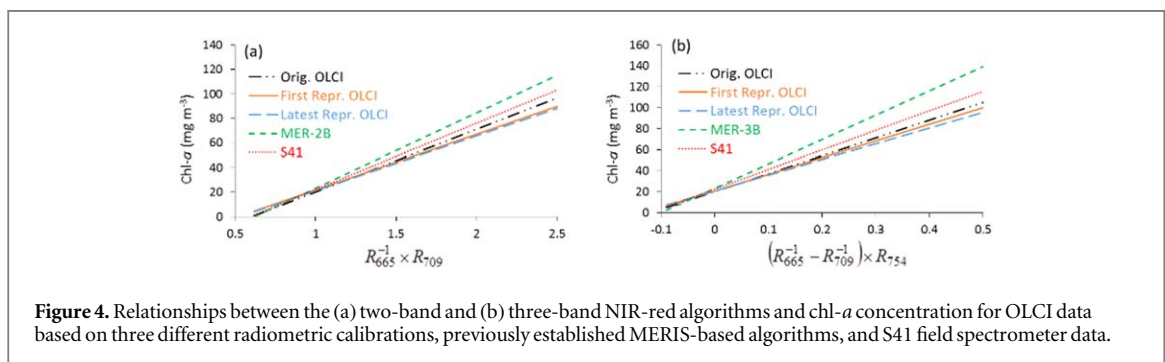
Figure 4. Relationships between the (a) two-band and (b) three-band NIR-red algorithms and chl-*a* concentration for OLCI data based on three different radiometric calibrations, previously established MERIS-based algorithms, and S41 field spectrometer data.

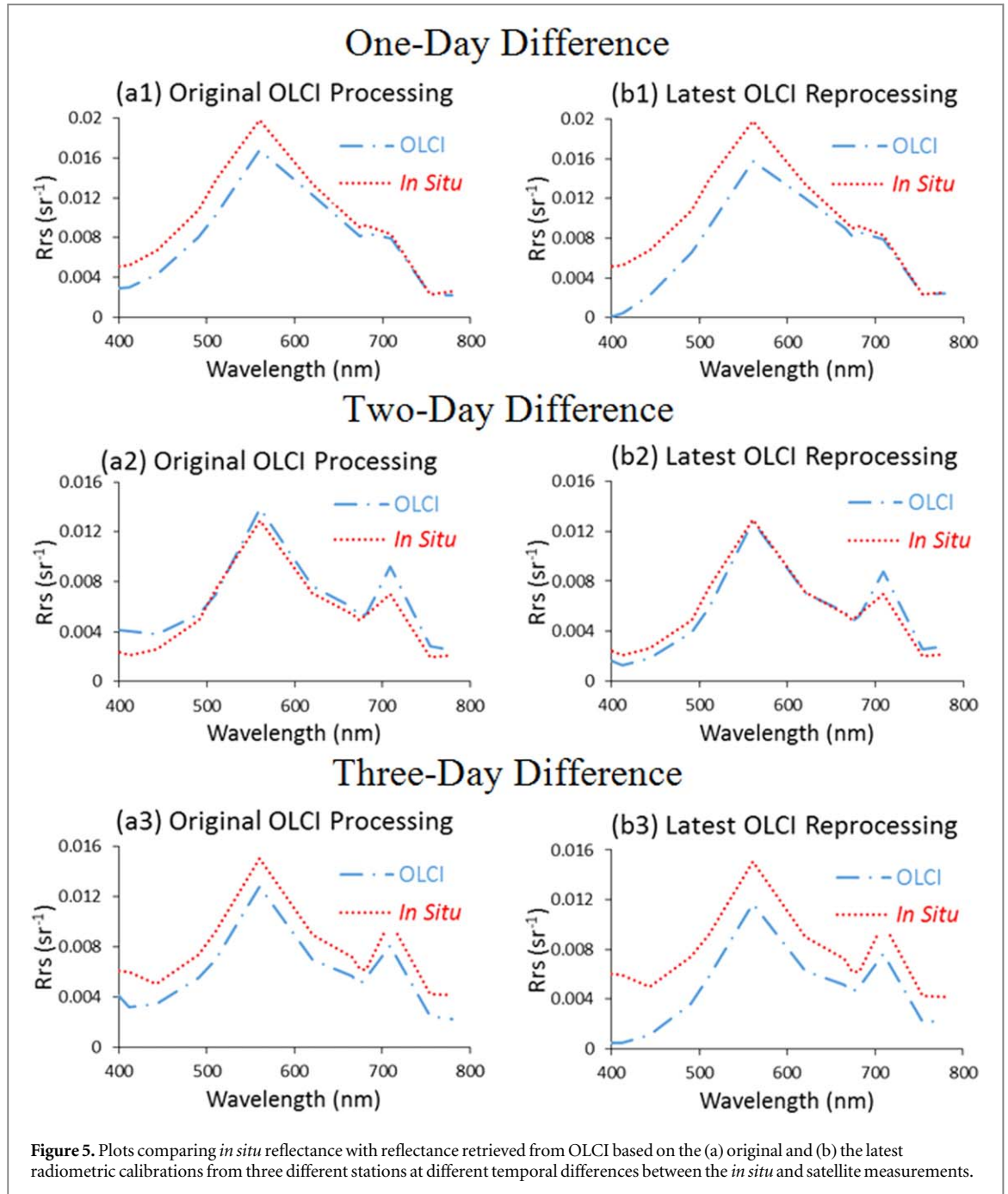Two-Band MERIS NIR-red Algorithm:
$$\text{Chl-}a = 61.324(R_{665}^{-1} \times R_{708}) - 37.94 \tag{6}$$

Three-Band MERIS NIR-red Algorithm:
$$\text{Chl-}a = 232.29[(R_{665}^{-1} - R_{708}^{-1}) \times R_{753}] + 23.174 \tag{7}$$

The MERIS-based algorithms exhibited a similar relationship with chl-*a* concentrations as did sensor-independent NIR-red algorithms that were developed based on radiative transfer modeling [11, 13]. Given that the characteristics of the MERIS and OLCI spectral channels used in the NIR-red algorithms are essentially the same and the atmospheric correction procedure applied is also the same, the difference in the coefficients are likely attributable to differences between the radiometric characteristics of MERIS and OLCI. Being a new sensor, the radiometric stability of OLCI is still under study and its radiometric calibration has been continually monitored and adjusted, with the calibration coefficients adjusted and the data reprocessed multiple times post-launch, as would be the case for any new sensor. With each reprocessing, the magnitude of the satellite-derived reflectance changes, which impacts the coefficients of the NIR-red algorithms. The results presented above are based on the latest reprocessing. For the data collected in June 2016, we had corresponding OLCI data in three versions of radiometric calibration—the original calibration implemented during the commissioning phase, the first reprocessing implemented in 2017, and the latest reprocessing implemented in 2018. Figure 4 shows the linear relationships of the NIR-red algorithms with chl-*a* concentration determined based on each of the three versions of OLCI data and the MERIS-based NIR-red algorithms for the June 2016 dataset. Also plotted is the relationship based on reflectance measurements from the S41 field spectrometer. As can be seen, each successive reprocessing of OLCI data has resulted in further deviation from the MERIS-based relationship, even though the OLCI-based algorithms are as close as or even closer to the relationship based on field spectrometer data than are the MERIS-based algorithms. Moreover, each successive reprocessing has resulted in further deviation from the field-spectrometer-based relationship as well. It must be noted very clearly that these results are simply presented as observations with no explicit or implicit intent to infer any conclusion about the quality or validity of successive radiometric calibrations of OLCI data. We do not suggest the use of NIR-red algorithms or any other derived product as a proxy for assessing the validity of radiometric calibration. However, it is worth noting the effects of radiometric calibration on the algorithms, especially if these algorithms are to be applied to data spanning long periods of time or data from multiple sensors.

OLCI-derived reflectances compared well with *in situ* reflectance measurements taken with the S41 field spectrometer (figure 5). The plots shown in figure 5 are typical of the comparisons obtained for 24 pairs of S41 and OLCI reflectance data, with the comparisons for some stations better and for others worse than what is

Figure 5. Plots comparing *in situ* reflectance with reflectance retrieved from OLCI based on the (a) original and (b) the latest radiometric calibrations from three different stations at different temporal differences between the *in situ* and satellite measurements.

shown. In cases where the comparison was worse, the spectra differed mostly only in magnitude, with the spectral shapes remaining similar. The reprocessing generally resulted in lower reflectance, especially in the short wavelengths. This decrease in the magnitude of reflectance is likely due to the application of vicarious gains in the reprocessing step by EUMETSAT (European Organisation for the Exploitation of Meteorological Satellites), the agency with operational responsibility over the Sentinel-3 mission. The vicarious gains, which were not applied to the original version of OLCI data, were applied in successive reprocessing steps to counter excessive brightness that was observed in the top-of-atmosphere data from the original calibration.

Spectral angle was used to further assess the comparison between the S41 and OLCI reflectance data. The spectral angle was calculated as,

$$\text{Spectral Angle} = \cos^{-1}\left(\frac{\sum_{i=1}^{nb} p_i r_i}{\sqrt{\sum_{i=1}^{nb} p_i^2}\sqrt{\sum_{i=1}^{nb} r_i^2}}\right) \quad (8)$$

where, nb is the number of wavelengths in the spectrum, p_i is the OLCI reflectance at the ith wavelength, and r_i is the corresponding S41 reflectance. The average spectral angle of separation between S41 and OLCI reflectance

IOP Publishing   *Environ. Res. Commun.* **1** (2019) 011002

▶▶ Letters

was progressively larger with each successive reprocessing, with the average spectral angle being 0.21 radians for the original processing, 0.27 radians for the first reprocessing, and 0.35 radians for the latest reprocessing. Nevertheless, the reflectance retrieved from OLCI generally compared quite well with S41 reflectance, thus demonstrating the validity of the radiometric calibration and the default atmospheric correction procedure currently implemented in the OLCI data processing scheme, at least in the context of using the reflectance in the red and NIR regions for estimating chl-*a* concentration.

4. Conclusion

The results presented demonstrate the potential for the use of OLCI data for monitoring water quality in turbid productive inland and coastal waters. The validity and stability of the coefficients of the OLCI-based NIR-red algorithms need to be tested with long-term data, especially as the radiometric calibration of the sensor is continually monitored and adjusted. Though differences in the results arising from the various versions of radiometric calibration of OLCI have been noted, these results are not meant to be used to draw any conclusion on the quality of a particular version of radiometric calibration. In spite of the anticipated launch of spaceborne hyperspectral sensors in the near future, multispectral algorithms such as the NIR-red algorithms, which were developed based on well-defined inherent spectral properties of water constituents, will continue to play a vital role in determining water quality from satellite data. With continued monitoring of the radiometric stability of the OLCI sensor and long-term acquisition of *in situ* data, robust NIR-red algorithms can be developed for operational estimation of chl-*a* concentration in inland and coastal waters using OLCI data.

ORCID iDs

Wesley J Moses ⓘ https://orcid.org/0000-0003-3551-6093

References

[1] Ryther J H and Yentsch C S 1957 The estimation of phytoplankton production in the ocean from chlorophyll and light data *Limnol. Oceanogr.* **2** 281–6

[2] Dall'Olmo G, Gitelson A, Rundquist D, Leavitt B, Barrow T and Holz J 2005 Assessing the potential of SeaWiFS and MODIS for estimating chlorophyll concentration in turbid productive waters using red and near-infrared bands *Remote Sens. Environ.* **96** 176–87

[3] Moses W J, Sterckx S, Montes M J, De Keukelaere L and Knaeps E 2017 Atmospheric correction for inland waters *Bio-optical Modeling and Remote Sensing of Inland Waters* ed D R Mishra, I Ogashawara and A A Gitelson (Amsterdam: Elsevier) pp 69–100 Chapter 3

[4] Sterckx S, Knaeps E and Ruddick K 2011 Detection and correction of adjacency effects in hyperspectral airborne data of coastal and inland waters: the use of the near infrared similarity spectrum *Int. J. Remote Sens.* **32** 6479–505

[5] Gitelson A, Dall'Olmo G, Moses W, Rundquist D, Barrow T, Fisher T, Gurlin D and Holz J 2008 A simple semi-analytical model for remote estimation of chlorophyll-a in turbid waters: validation *Remote Sens. Environ.* **112** 3582–93

[6] Matthews M W 2011 A current review of empirical procedures of remote sensing in inland and near-coastal transitional waters *Int. J. Remote Sens.* **32** 6855–99

[7] Odermatt D, Gitelson A, Brando V E and Schaepman M 2012 Review of constituent retrieval in optically deep and complex waters from satellite imagery *Remote Sens. Environ.* **118** 116–26

[8] Gurlin D, Gitelson A A and Moses W J 2011 Remote estimation of chl-*a* concentration in turbid productive waters—return to a simple two-band NIR-red model? *Remote Sens. Environ.* **115** 3479–90

[9] Yacobi Y Z, Moses W J, Kaganovsky S, Sulimani B, Leavitt B C and Gitelson A A 2011 NIR-red reflectance-based algorithms for chlorophyll-a estimation in mesotrophic inland and coastal waters: lake Kinneret case study *Wat. Res.* **45** 2428–36

[10] Moses W J, Gitelson A A, Perk R L, Gurlin D, Rundquist D C, Leavitt B C, Barrow T M and Brakhage P 2012 Estimation of chlorophyll-*a* concentration in turbid productive waters using airborne hyperspectral data *Wat. Res.* **46** 993–1004

[11] Gilerson A, Gitelson A, Zhou J, Gurlin D, Moses W, Ioannou I and Ahmed S 2010 Algorithms for remote estimation of chlorophyll-a in coastal and inland waters using red and near infrared bands *Opt. Exp.* **18** 24109–25

[12] Moses W J, Gitelson A A, Berdnikov S and Povazhnyy V 2009 Satellite estimation of chlorophyll-*a* concentration using the red and NIR bands of MERIS—the Azov Sea case study *IEEE Geosci. Remote Sens. Lett.* **4** 845–9

[13] Moses W J, Gitelson A A, Berdnikov S, Saprygin V and Povazhnyi V 2012 Operational MERIS-based NIR-red algorithms for estimating chlorophyll-*a* concentrations in coastal waters—the Azov sea case study *Remote Sens. Environ.* **121** 118–24

[14] Moses W J, Gitelson A A, Berdnikov S, Bowles J H, Povazhnyi V, Saprygin V, Wagner E J and Patterson K W 2012 HICO-based NIR-red models for estimating chlorophyll-*a* concentration in productive coastal waters *IEEE Geosci. Remote Sens. Lett.* **11** 1111–5

[15] Mollaee S 2018 Estimation of phytoplankton chlorophyll-*a* concentration in the western basin of Lake Erie using Sentinel-2 and Sentinel-3 data *Master's Thesis* University of Waterloo, Ontario, Canada

[16] Toming K, Kutser T, Uiboupin R, Arikas A, Vahter K and Paavel B 2017 Mapping water quality parameters with Sentinel-3 Ocean and Land Colour Instrument imagery in the Baltic *Sea Rem. Sens.* **9** 1070 21

[17] Smith M E, Robertson Lain L and Bernard S 2018 An optimized chlorophyll *a* switching algorithm for MERIS and OLCI in phytoplankton-dominated waters *Remote Sens. Environ.* **15** 217–27

[18] Borysova O, Kondakov A, Paleari S, Rautalahti-Miettinen E, Stolberg F and Daler D 2005 Eutrophication in the Black Sea region: impact assessment and causal chain analysis *Global Int. Wat. Assess.* University of Kalmar, Sweden

[19] Matishov G 2005 System approach to the water quality and bioproductivity of the Azov Sea basin *River Basin Management III WIT Trans. Ecology and Environ.* ed C A Brebbia vol 83 (Southampton: WIT Press) pp 347–57

[20] Shokhin I V, Nabozhenko M V, Sarvillina S V and Titova E P 2006 The present-day condition and regularities of the distribution of the bottom communities in Taganrog Bay *Oceanology* **46** 401–10

[21] Jeffrey S W and Humphrey G F 1975 New spectrophotometric equations for determining chlorophylls a, b, c1, c2 in higher plants, algae, and natural phytoplankton *Biochem. Physiolo. Pflanzen* **167** 191–4

[22] Mueller J L *et al* 2003 Ocean optics protocols for satellite ocean color sensor validation, revision 4, volume III: radiometric measurements and data analysis protocols *NASA Tech. Memo NASA/TM-2003-21621/Rev-Vol III*

[23] Mobley C D 1999 Estimation of the remote sensing reflectance from above-surface measurements *Appl. Opt.* **38** 7442–55

[24] Moore G F, Aiken J and Lavender S J 1999 The atmospheric correction of water colour and the quantitative retrieval of suspended particulate matter in case II waters: application to MERIS *Int. J. Remote Sensing.* **20** 1713–33

[25] Aiken J and Moore G 2000 ATBD case 2 s bright pixel atmospheric correction, center for coastal & marine sciences, plymouth marine *Laboratory, U.K. Rep.* PO-TN-MEL-GS-0005 14 p

[26] Albers V M and Knorr H V 1937 Absorption spectra of single chloroplasts in living cells in the region from 664 mμ to 704 mμ *Plant Phys.* **12** 833–43

[27] Vasilkov A and Kopelevich O 1982 Reasons for the appearance of the maximum near 700 nm in the radiance spectrum emitted by the ocean layer *Oceanology* **22** 697–701

[28] Gitelson A 1992 The peak near 700 mm on radiance spectra of algae and water - relationships of its magnitude and position with chlorophyll concentration *Int. J. Remote Sens.* **13** 3367–73

[29] Dall'Olmo G and Gitelson A A 2005 Effect of bio-optical parameter variability on the remote estimation of chlorophyll-a concentration in turbid productive waters: experimental results *Appl. Opt.* **44** 412–22